Characterization of a 13.5nm Source for EUV Lithography based on a Dense Plasma Focus and Lithium Emission

Igor Fomenkov[a], William Partlo[a], Daniel Birx[b]

[a]Cymer Inc., 16750 Via Del Campo Crt., San Diego, CA 92127

[b]Applied Pulse Power Technologies Inc., 3300 Crismore Lane, Oakley, CA 94561

Submitted to: Sematech International Workshop on Extreme Ultraviolet Lithography, 1999.

ABSTRACT

Recent investigations of a Dense Plasma Focus (DPF) device in combination with the 13.5nm Lihium emission line have shown that this technology has promise as a useful light source for EUV lithography. Initial characterization efforts found that significant amounts of EUV radiation can be produced. For example, the prototype DPF converts 25J of stored electrical energy into 0.76J of in-band 13.5nm radiation into 4π steradians. The major drawback found with this prototype was poor position stability leading to large integrated source size and high electrode erosion.

Modifications of this prototype DPF have resulted in a system that exhibits greatly improved stability and much lower input energy requirements. Stable operation can now be achieved with as little as 3J of stored electrical energy. EUV images taken with a pinhole camera show an integrated source size of 300-400μm diameter FWHM. Source size and stability was found to be acceptable for pulse repetition rates up to the power supply limit of 2500Hz.

Initial characterization of the optical performance of a prototype grazing incidence collector has also been completed. This optic is critical for long term use of the Lithium based DPF because of its expected tolerance to Lithium vapor. Measurements of the near field and far field performance of this prototype collector show that wave front errors introduced by several of the reflecting parabolic shells increase the effective divergence of a 500μm diameter source by a factor of two.

Keywords: EUV Lithography, Dense Plasma Focus, Solid State Pulse Power, Lithium Emission

1. INTRODUCTION

One of several critical technologies required for practical implementation of EUV lithography is a reliable, high brightness EUV light source with emission characteristics well matched to the reflection band of the Mo/Si or Mo/Be mirror systems. Since the proposed all-reflective EUV lithography tools are slit scanning based systems, such an EUV light source must also exhibit high repetition rate capability. In addition to these requirements, a practical EUV light source must operate debris-free or employ an effective debris mitigation strategy.

A Dense Plasma Focus (DPF) device has been investigated as a source for EUV lithography because of its potential for high source brightness and high repetition rate operation. A prototype DPF has been constructed that employs an all-solid-state pulse power drive system. This prototype DPF is based on the development work done toward an efficient electric plasma thruster for space applications[1-3]. Initial characterization of this prototype showed that it was relatively efficient at converting stored electrical energy into in-band EUV radiation. For example, with 25J input this prototype emitted 0.76J into the 13.5nm doubly ionized Lithium line (4π steradians) for a conversion efficiency of 3%[4].

The negative aspects of this prototype's performance were poor stability and high input energy, leading to excessive electrode erosion and limited pulse repetition rate capability. Efforts over the last 6 months have concentrated on producing a small and stable plasma region while minimizing the required input energy. If a well controlled DPF can be produced with an input

energy of 5J or less then high pulse repetition rate operation between 1kHz and 3kHz would be feasible since the average heat load in the electrode region would be 5kW to 15kW.

Also critical to the success of this EUV source concept is the use of a collection optic tolerant to the presence of Lithium vapor. To achieve maximum in-band emission efficiency, the DPF source will contain Lithium vapor. Lithium has a strong, narrow emission line at 13.5nm from its doubly ionized state. A multi-layer mirror fabricated from Mo/Si layers is not expected to survive long in the presence of Lithium vapor, so a grazing incidence collector design has been chosen for the primary collection optic. The prototype of this grazing incidence optic has been fabricated. Testing with visible light shows that imperfections in several of the collector's parabolic surfaces introduce wave front errors sufficient to increase the source divergence of a 500μm source by a factor of two.

2. DENSE PLASMA FOCUS SYSTEM DESCRIPTION

A DPF device consists of a coaxial electrode set driven to a voltage potential difference that results in the formation of a conductive plasma sheath between the inner and outer electrodes. Typical DPF systems operate in the range of 10-50kV between electrodes resulting in large stored energies in the drive capacitor. Careful design of the drive inductance enables operation of this prototype DPF below 1kV.

Fig 1 shows a simplified diagram of the electrical drive circuit. The initial storage capacitor, C_0, is charged on command by the DC power supply. Once full charge is reached, the IGBTs are triggered into conduction causing resonant transfer of energy from C_0 to C_1. The initial prototype system possessed a C_1 capacitor of 65μF. Modifications of this prototype have resulted in a reduction in C_1 to 21.7μF and thus a factor of three reduction in stored energy for the same operating voltage.

Once peak voltage on C_1 is reached, a set of hollow cathode pre-ionization sources (not shown in Fig 1) are energized to initiate avalanche break down in the gas between the inner and outer electrodes. The low inductance of the drive circuit ensures a rapid rise in current flow and the application of nearly all of the C_1 voltage across the electrode set.

Once significant current begins to flow through the plasma sheath, **J** X **B** forces accelerate the plasma away from the base of the electrode set and toward the end of the anode. The flow of electrons and ions as well as the magnetic field and resulting force vector are shown in Fig 2. Simultaneous with the acceleration of the plasma, the current flowing from C_1 through the series combination of the drive inductance and electrode inductance rises toward a maximum. The plasma sheath is eventually driven off the end of the anode resulting in magnetic forces that compress the gas in this region toward the central axis as shown in Fig 3. Compression and heating raises the temperature of the ions in this region to levels sufficient for intense emission in the EUV spectral region.

3. SPECTRAL MEASUREMENTS

Since the Mo/Si mirror systems exhibit high reflectivity only over a narrow band of wavelengths, detailed measurements of the emission spectrum from this prototype DPF are needed to quantify the useable radiation. By placing a small amount of Lithium on the tip of the anode, the emission spectrum can be recorded and we can determine if the DPF produces a plasma temperature appropriate for production of EUV radiation. Lithium has been proposed as an emission source for EUV lithography because of its narrow spectrum and intense emission into wavelengths well matched to the reflectance band of Mo/Si mirrors[5].

Fig 4 shows the measured emission spectrum of the DPF Lithium plasma over a range from 10nm to 24nm. Also shown on this graph is the published reflectivity of a typical Mo/Si mirror. The Lithium emission lines between 10nm and 14nm are due to electronic transitions of doubly ionized Lithium, also referred to as Hydrogen-like Lithium. Verifying the wavelength calibration of the spectrometer is simplified by the fact that the Hydrogen-like Lithium lines are narrow and well known. Using this experimental setup, we can locate six electronic transitions of doubly ionized Lithium as shown in Fig 5. The absence of any strong lines above the 2p-1s transition of doubly ionized Lithium is a particular advantage of Lithium as an EUV emission source. As the Lithium plasma is heated to high temperatures, there are no effective radiative cooling channels above the 13.5nm line. A substantial portion of the radiated energy will be emitted in the 13.5nm line because it is a highly probable transition and each photon carries much more energy than longer wavelength transitions.

The theoretical quantum efficiency for the 13.5nm line can be calculated by dividing the energy of the 2p-1s transition into the sum of the 2p-1s transition energy and the energy required to form doubly ionized Lithium. The literature states that the energy required to doubly ionize Lithium is 81eV[6]. Thus the theoretical quantum efficiency for 13.5nm emission is 53%.

As shown in Fig 4, the 13.5nm Lithium emission line matches well to the Mo/Si reflectance band. A finer resolution spectral scan centered on 13.5nm is shown in Fig 6 along with the published reflectivity of a Mo/Si mirror. The measured bandwidth for this 13.5nm emission line is 0.03nm. It is thought that this result may be spectrometer resolution limited and the bandwidth of this emission line is likely less than 0.03nm. Fortunately, the exact bandwidth of this emission line is unimportant to the operation of the Mo/Si mirror since even the measured 0.03nm result is much more narrow than the reflectance bandwidth of the Mo/Si mirror.

4. SOURCE SIZE MEASUREMENTS

Once the capability of the DPF to produce high plasma temperatures was verified, efforts were concentrated on improving stability and reducing the required input energy. Since the DPF is operated with a background gas of Argon and our Lithium vapor delivery techniques are immature, the following characterization efforts were performed with Argon only. Fortunately, Argon does possess emission lines in the EUV region so EUV pinhole images can be taken of various configurations.

The first step toward a better understanding of the DPF instabilities was to take visible wavelength gated camera images of the plasma formation. Fig 7 shows a time sliced sequence of the DPF formation with a solid anode (center electrode). Each frame is an average of 10 images taken in 200ns steps. The initial frames show the run down phase with the main DPF forming during the 600ns frame. Following formation of the DPF, the plasma sheath continues to travel axially until it completely detaches from the anode. One can also see emission from the anode itself due to excessive heating caused by direct contact with the hottest portion of the plasma.

The hot spot formation on the tip of the electrode is easily solved by switching to a hollow anode. The formation of the DPF with a hollow anode is shown in Fig 8. Again the frames are an average of 10 images each taken in 200ns steps. As with the solid anode, the plasma sheath continues its axial travel after formation of the DPF. Though no excessive heating of the anode is observed since there is no solid material near the hottest portions of the plasma, there still remains the problem of unstable operation due to the plasma detaching from the anode.

The detachment problem was addressed by additional modifications to the electrode configuration. These changes resulted in repeatable formation of a small and stable region of hot plasma centered on axis with the hollow anode. Unfortunately, this latest configuration contains components that prevent side-on viewing and thus taking gated camera images of DPF formation is not possible. Instead we rely on EUV pinhole camera images taken along the axis to verify source size and stability.

The pinhole camera arrangement that we employed is shown in Fig 9. A 50μm pinhole located on axis 25cm from the tip of the anode is used to form an image on a back-side illuminated CCD array located 32cm from the pinhole. Spectral filtering is provided by a 1μm thick Beryllium foil placed just behind the pinhole. The published transmission of this foil is shown in Fig 10. The spatial resolution of this pinhole camera is limited by both geometry of the pinhole and diffraction at the pinhole. The resulting convolution of the geometric and diffraction spot sizes is shown in Fig 11 giving a system resolution of 92μm under the assumption of 13.5nm illumination.

An EUV source image taken while operating at 10Hz with a buffer gas of Argon is shown in Fig 12. The resulting source size is 313μm FWHM. The vertical stripe seen in the false color two dimensional image is due to a row of damaged pixels on the CCD array. This image was taken with a 90 second exposure while operating continuously at 10Hz, so 900 pulses were integrated on the array to form this image. The resulting small integrated source size demonstrates that the EUV source is both small and highly stable in its location.

The size of the hot plasma indicated by EUV emission can be compared to the dimensions of the hollow anode. Fig 13 shows the measured EUV source size on the same scale as the anode's inner and outer radii.

5. REPETITION RATE SCALING

One promising feature of this DPF device is its proven high repetition rate capability when used as an electric plasma thruster for space applications[1-3]. As a plasma thruster, short bursts of 3,000Hz operation are routinely demonstrated. To investigate the repetition rate performance of this DPF device as an EUV source, we operated at increasing repetition rates in short bursts while taking EUV pinhole camera images.

Fig 14 shows the measured EUV source profiles for repetition rates from 10Hz to 1000Hz. As the repetition rate is increased up to 1000Hz the source brightness actually increases, that is the source size remains the same or smaller while the total EUV output increases. EUV images were taken up to the DC power supply limit of 2500Hz. The measured source profile for 2500Hz is shown in Fig 15 along with the 1000Hz result for comparison. The integrated source size for 2500Hz is slightly larger than for 1000Hz, but the total emission is higher for 2500Hz. A summary of the measured EUV source size and total EUV emission is plotted in Fig 16. The total EUV emission monotonically increases with repetition rate while the integrated source size remains below 300μm up to 1500Hz, after which it begins to increase reaching 410μm at 2500Hz.

It is not known for certain the cause of the increase in total EUV emission with increasing repetition rate. One possibility that suggests itself is the presence or absence of contaminants "boiled" off from surfaces during previous pulses. As the period between pulses decreases with higher repetition rate, these contaminants have less time to re-condense. One attribute of this prototype's performance that supports the idea of contaminate interactions is a 30 minute "warm-up" characteristic exhibited by this machine. Even after maintaining vacuum for more than a week and running for greater than 10^6 pulses, the total EUV emission goes through a transient period of approximately 30 minutes upon restart after no running for several hours. Fig 17 shows the measured EUV source size and total EUV emission while operating at 10Hz after an off period of 15 hours. Both the measured size and emission go through a 30 minute transient. This characteristic repeats itself after each extended off period.

This prototype was constructed without any special cleaning or handling procedures and the vacuum pump is a two stage rotary pump used without a fore-line trap. For future machines, much greater attention will be given to material choices, parts handling, and clean vacuum technology.

6. GRAZING INCIDENCE COLLECTOR

As important as creating an EUV source with high spectral brightness is collecting and relaying this radiation to a region safe for use with the sensitive Mo/Si EUV mirrors. Since this DPF source will use Lithium vapor as its emission specie, some background level of Lithium vapor is expected to be near the primary collection optic. Mo/Si multi-layer EUV mirrors are expected to degrade under exposure to Lithium vapor so an alternate collection optic is required. Use of a collector based on grazing incidence reflections offers promise because such an optic exhibits high reflectivity and can be fabricated from materials inert to Lithium vapor exposure.

The multiple shells of the prototype grazing incidence collector was fabricated with Nickel shells coated with Palladium. Fig 18 shows the published reflectivity versus angle for various candidate coating materials. From these curves one can see that Molybdenum exhibits superior reflectivity up to 20° grazing incidence. In fact, if a grazing incidence collector were fabricated using a Molybdenum coating with grazing incidence angles no greater than 20° it would have higher efficiency than a multi-layer EUV mirror with equivalent collection angle.

Palladium was chosen as the coating material for this prototype because the vendor, Parallax Research Inc., had extensive experience with Palladium coatings[7]. Because of the reduced reflectivity of Palladium at higher grazing incidence angles, the design criteria for this optic was for a single reflection and grazing incidence angle no greater than 10°. A summary of the design criteria are given in the following table:

Collector Output:	Collimated Beam
Output Beam Diameter:	50mm
Distance to Entrance:	45mm
Number of Shells:	5

Grazing Angle:	<10°
Collector Length:	65mm
Reflecting Coating:	Palladium
Collection Angle:	40°
Solid Angle:	0.38 Sterad (0.34NA)

While this prototype optic operates at an impressive sounding 0.34NA, it collects only 6% of the available 2π solid angle. A CAD rendering of this optic is shown in Fig 19. The cut away view shows the five nested shells.

Visible light testing of this optic was performed both in the far field and near field. The optical setups for these tests are shown in Fig 20. The output from a 50μm diameter fiber was used to simulate point source illumination with an illumination angle sufficient to fill the full collection angle of the optic under test. For far field measurements, a conventional lens with f=300mm was used to focus the collimated output from the test optic onto a CCD array placed at the focal plane of the f=300mm lens. For the near field measurements, an aperture was placed at the focal plane of the f=300mm lens and the camera and lens were positioned to form an image of the collector's exit aperture on the CCD array.

The measured far field pattern for this prototype optic is shown in Fig 21. The upper left corner intensity plot shows the performance of the entire optic with a FWHM divergence of 1.8mrad and a FW90% divergence of 5.0mrad. The remaining five intensity plots show the far field pattern created by each of the five individual shells (Refl. 1 being the outer most shell and Refl. 5 the inner most). These measurements show that the outer most shell exhibits worse performance than the inner shells.

The measured near field performance is shown in Fig 22. The lower left intensity plot is shows the illumination at the exit of the collector with no aperturing at the focal plain of the f=300 lens. The shadowing from the support spokes and the finite thickness of the shells can be seen. The remaining three intensity plots were recorded with an aperture placed at the focal plane of the f=300mm lens. The aperture is made smaller from left to right (10mrad down to 3.3mrad). As the aperture size is reduced, and thus higher divergence angles rejected, the near field pattern becomes dim in the regions were the shells deviate from their desired shape. The outer most shell shows the worst wave front errors and the second most outer shell also shows some imperfections.

Since this optic will be used to collect light from a small but extended source, we tested its performance when illuminated by a 500μm diameter fiber bundle. The resulting far field divergence is shown in Fig 23 along with the simulated divergence from this source size assuming a perfect optic of this type. This prototype optic increases the theoretical divergence by a factor of two.

7. NEAR TERM IMPROVEMENTS

Now that a small and stable plasma has been demonstrated with input energies less than 5J, a method for introducing Lithium vapor must be developed so that the DPF will radiate efficiently within the spectral region of the Mo/Si multi-layer mirrors. Such development is currently underway with a simple demonstration capability expected early next year.

Further investigations of basic DPF performance will continue with upgrades to the power system to enable 5000Hz operation. Cleanliness and appropriate material choices will be implemented to eliminate possible uncontrolled plasma constituents besides the desired Argon and Lithium. Though very little thermal engineering has been performed to date, the prototype will be operated at higher average powers to explore the limits of the present design so that a well directed thermal effort can be begun.

A second generation grazing incidence collection optic will be fabricated with several improved features. The collection angle will be increased so that twice the solid angle is collected, making this optic a better match for the proposed 0.25NA EUV imaging systems and increasing the total collection efficiency. The form this optic will also be changed from a parabolic collimator to and ellipsoidal imager. Instead of creating a 50mm diameter collimated beam of EUV radiation, this optic will image the source to a small point more appropriate for our intended Lithium protection strategies.

And finally, a long term life test of the present configuration will be initiated. This test configuration may not reflect the exact details of a final design, but general knowledge of erosion rates and failure modes early in the development cycle should be useful.

8. CONCLUSIONS

Initial characterizations of this prototype DPF have shown that it can produce lithographicaly significant amounts of radiation with a spectrum well matched to the Mo/Si EUV mirror systems. The latest experimental work has shown that a small and stable plasma can be formed with input energies less than 5J. Combining the efficient emission of Lithium with the high repetition rate, small source size of the latest DPF prototype should lead to a source with sufficient in-band power to be worthy of consideration for production prototype EUV lithography tools.

Long condenser life depends on successful implementation of a debris mitigation strategy based on the use of a grazing incidence primary collection optic. The wave front quality of the first prototype grazing incidence collector needs a factor of two improvement, but the issues leading to poor wave front quality seem to be understood and efforts are under way to reduce these effects in the next prototype.

REFERENCES

1. J. Ziemer, E. Cubbin, E. Choueiri, and D. Birx, "Performance Characterization of a High Efficiency Gas-Fed Pulsed Plasma Thruster," *33rd AIAA/ASME/SAE/ASEE Joint Propulsion Conference,* Seattle, WA, 1997.

2. J. Ziemer, E. Choueiri, and D. Birx, "Trends in Performance Improvements of a Gas-Fed Pulsed Plasma Thruster," *25th International Electric Propulsion Conference,* Cleveland, OH, 1997.

3. D. Birx, "Plasma Gun and Methods for the use Thereof," *US Patent 5,866,871,* Feb. 2, 1999.

4. W. Partlo, I. Fomenkov, D. Birx, "EUV (13.5nm) Light Generation Using a Dense Plamsa Focus Device," *SPIE Proc. on Emerging Lithographic Technologies III*, Vol. 3676, pp 846-858, March, 1999.

5. M. Klosner and W. Silfvast, "Feasibility of Various Discharge Configurations for High Intensity Lithium Vapor Discharge Source at 13.5nm for EUVL," *OSA TOPS on Extreme Ultraviolet Lithograph*, Vol. 4, May, 1996.

6. W. Silfvast, "Efficient Narrow Spectral Width Soft-X-Ray Discharge Sources," *US Patent 5,499,282*, Mar., 1996.

7. D. Ohara, "Fabrication of Collection Optics for 13nm Radiation," *Quotation submitted to Cymer,* Aug., 1998.

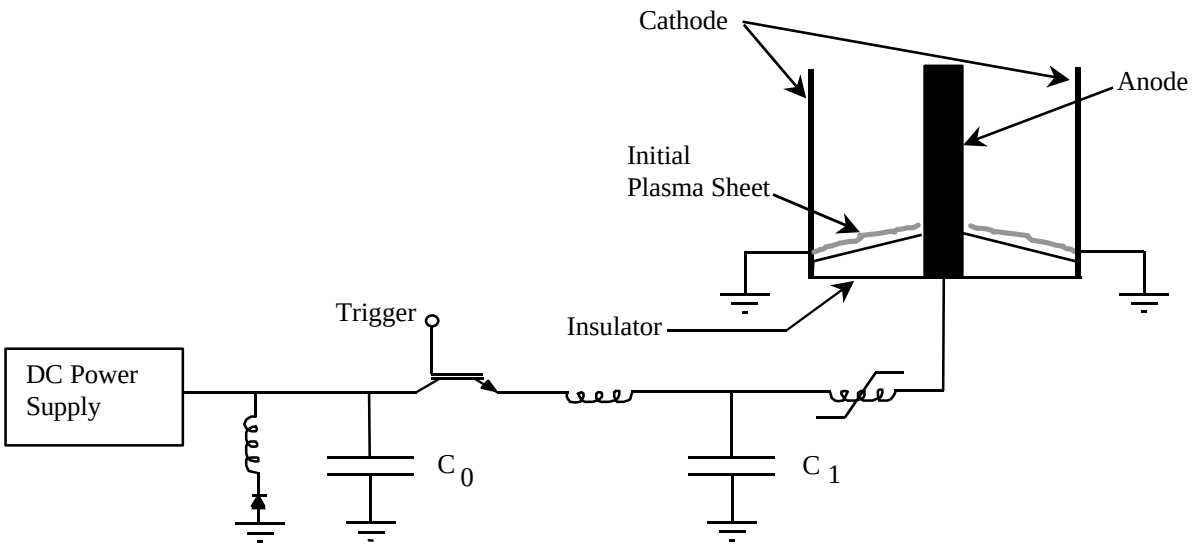

Fig 1 Simplified diagram of electrical drive circuit and DPF electrode set.

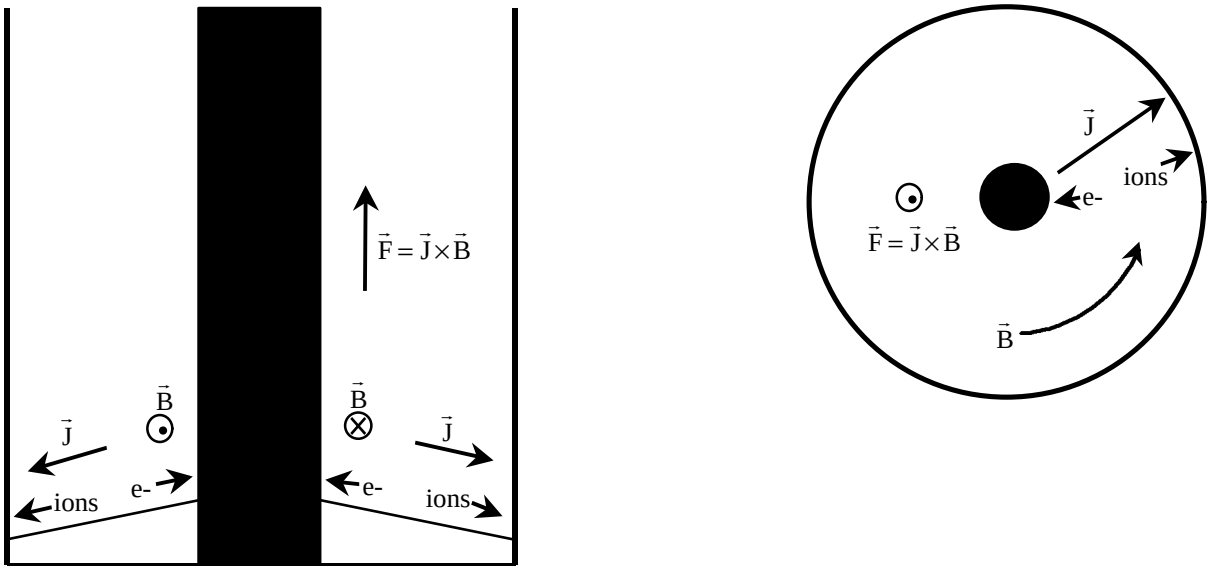

Fig 2. Electron and Ion current flow and resulting force vector in plasma sheath.

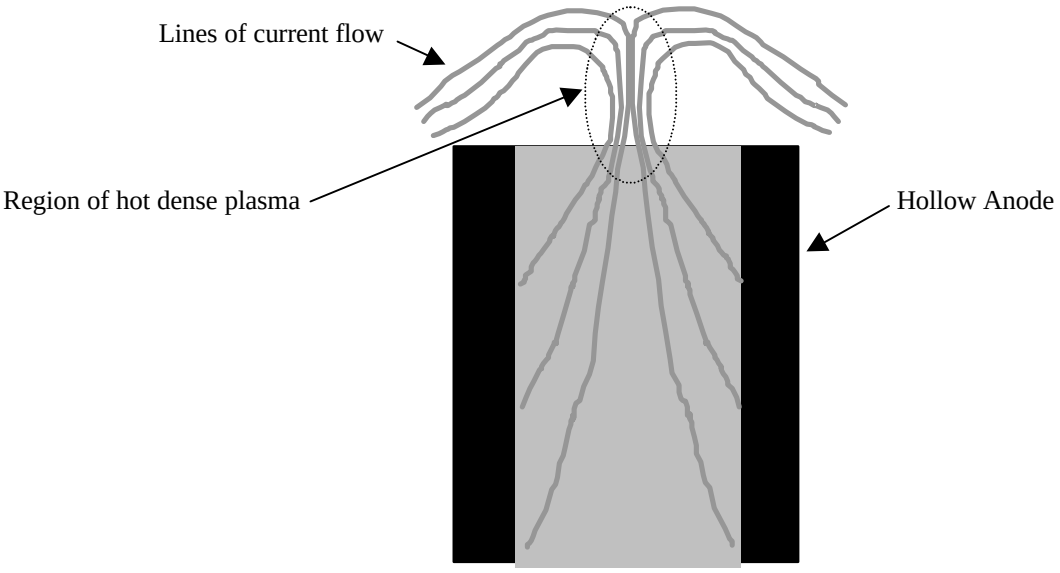

Fig 3. Compression and heating of gas located near tip of anode as plasma sheath accelerates off end of anode.

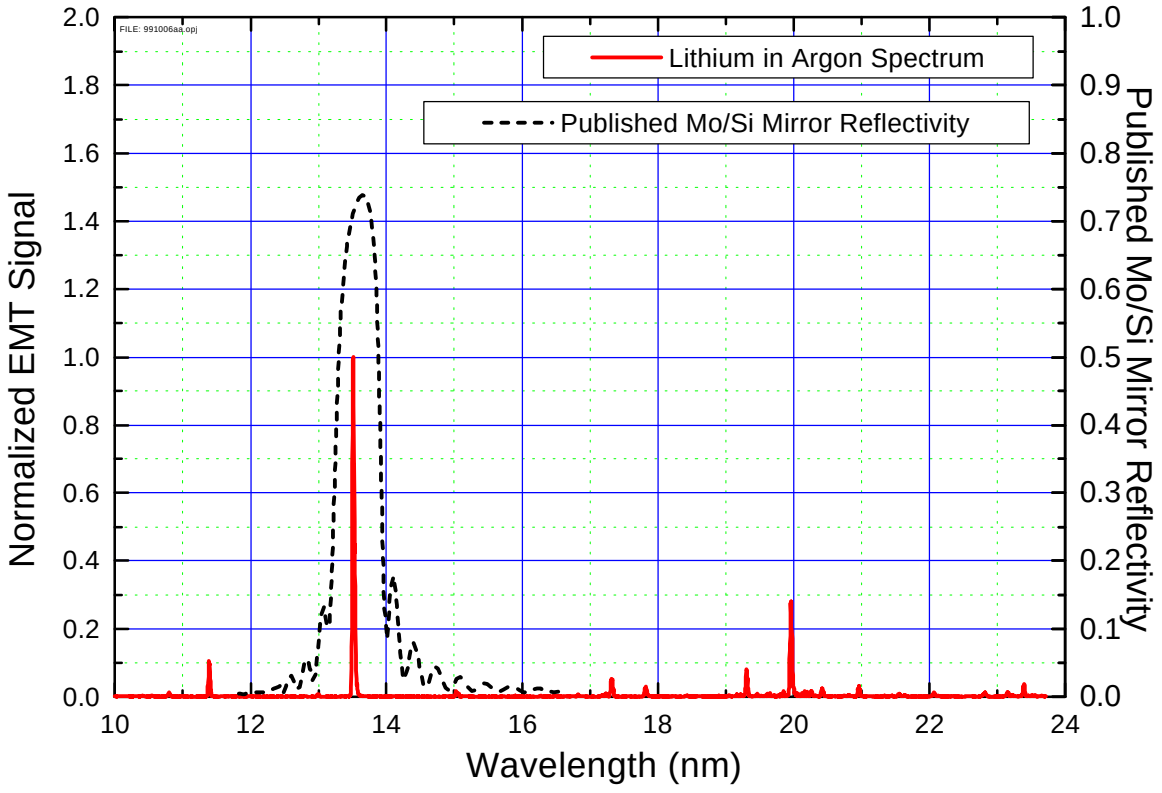

Fig 4. Measured emission spectrum of the DPF Lithium plasma over a range of 10nm to 24 nm.

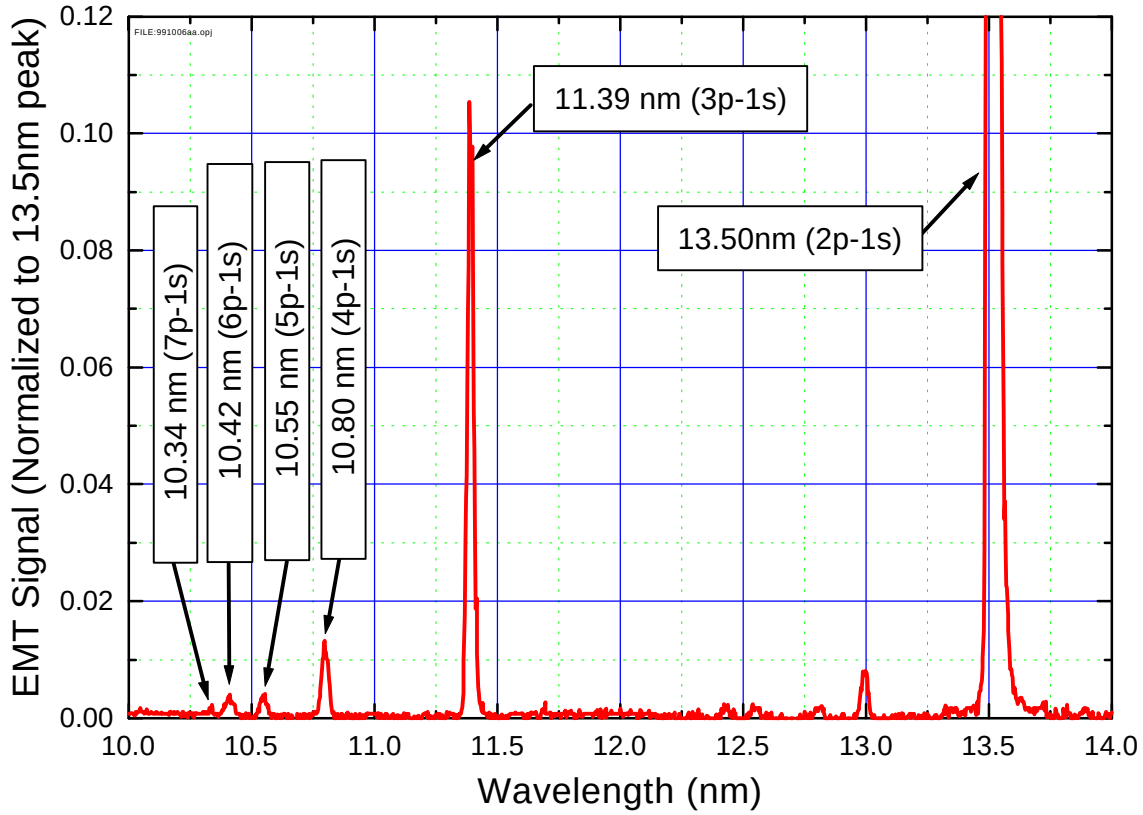

Fig 5. Measured emission of 6 electronic states of doubly inoized Lihtium.

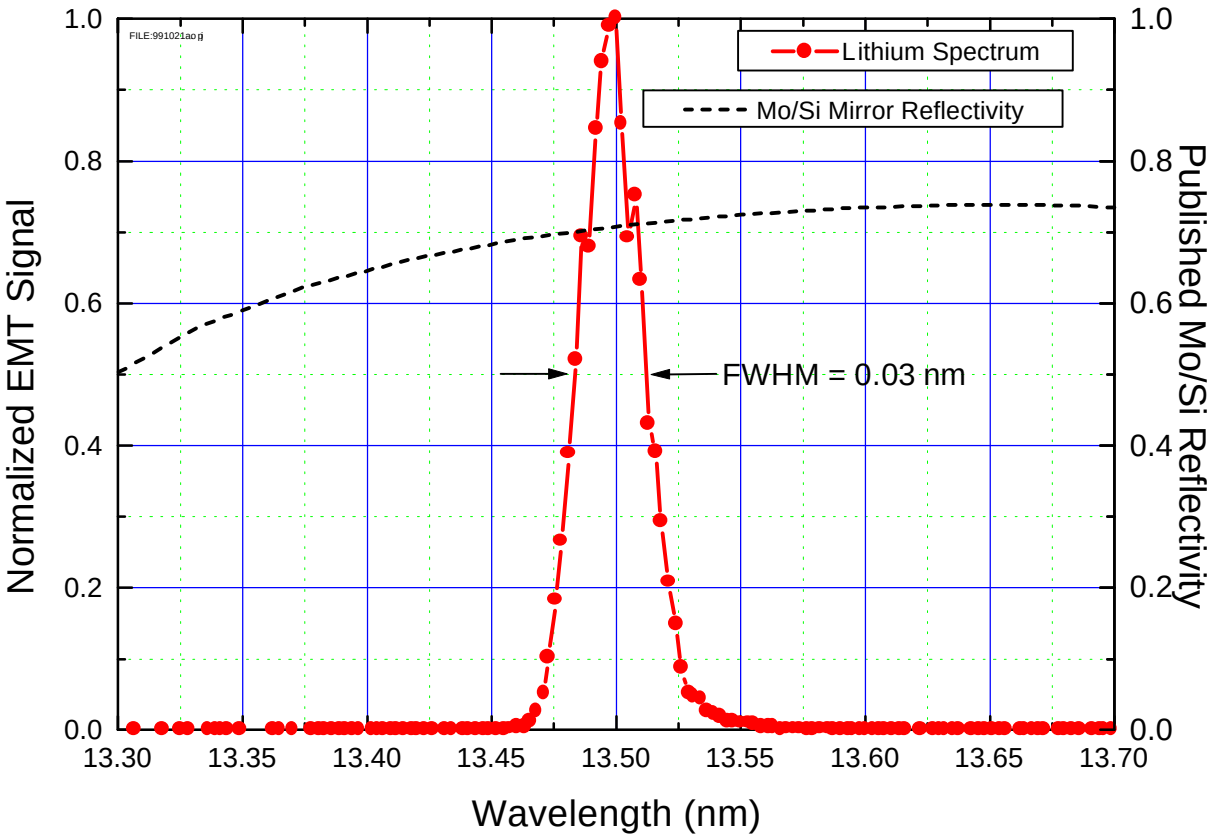

Fig 6. Fine resolution spectrum of the 13.5nm emission line of doubly ionized Lithium.

Fig 7. Side-on visible gated camera images of DPF with solid anode

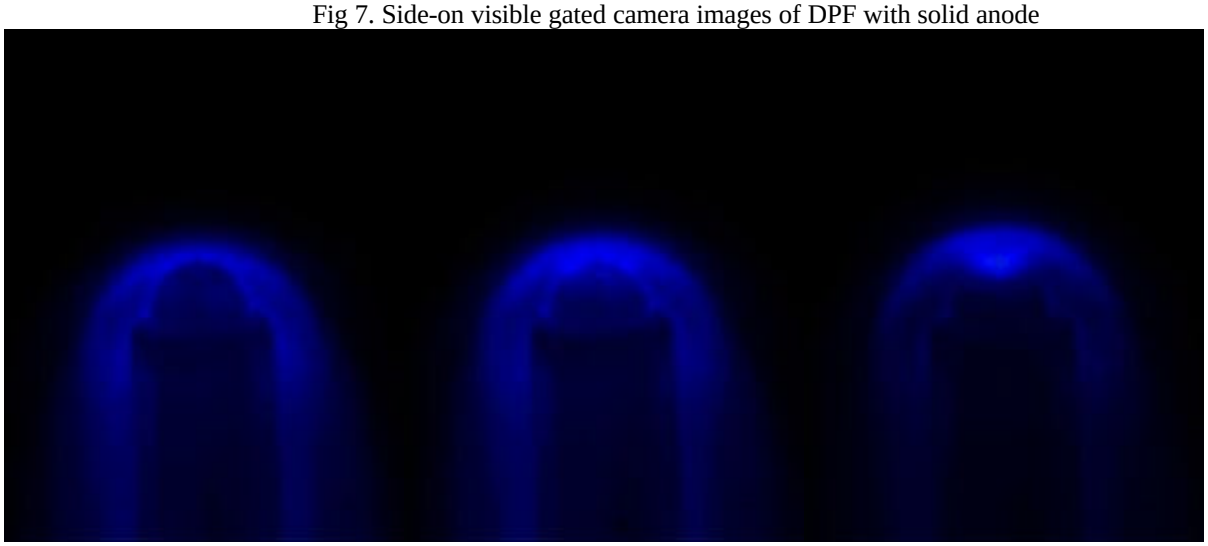

t=0ns t=200ns t=400ns

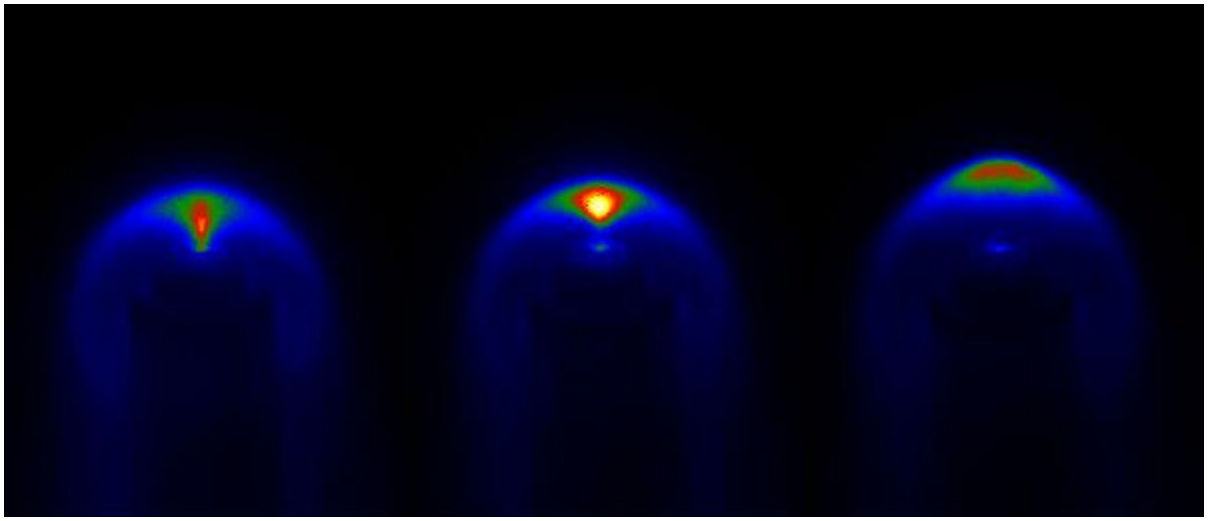

t=600ns t=800ns t=1000ns

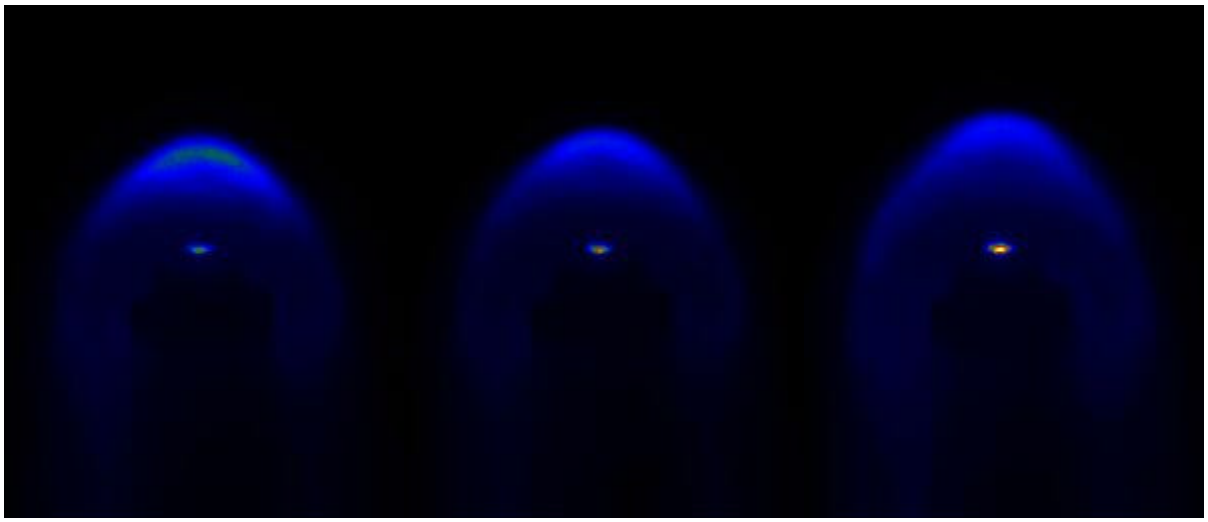

t=1200ns t=1400ns t=1600ns

Fig 8. Side-on visible gated camera images of DPF with hollow anode.

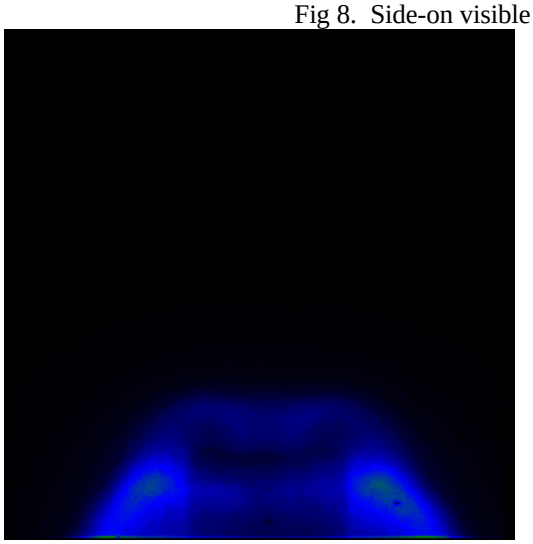

t=0ns

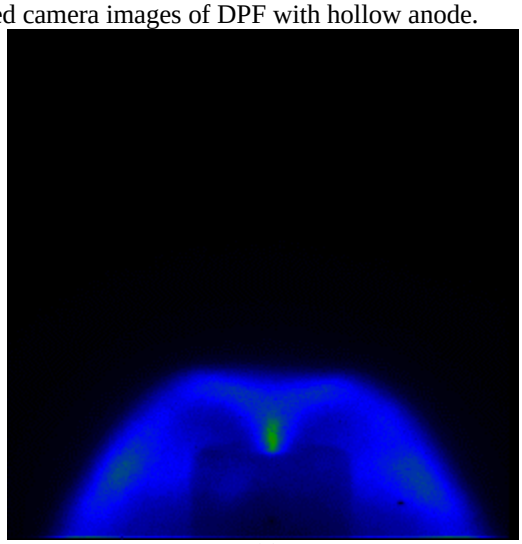

t=200ns

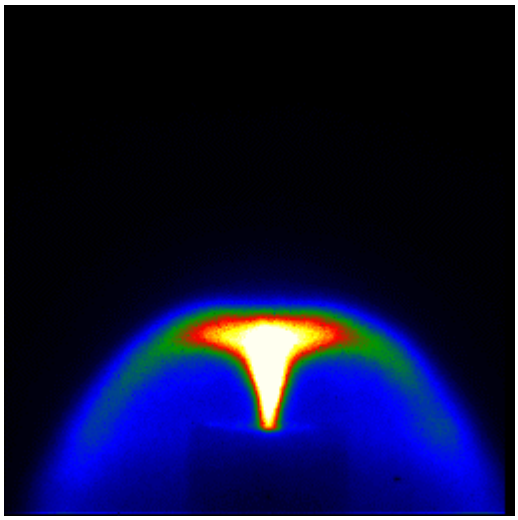

t=400ns

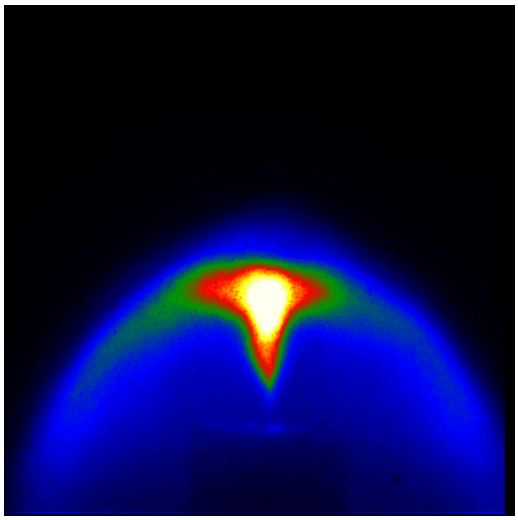

t=600ns

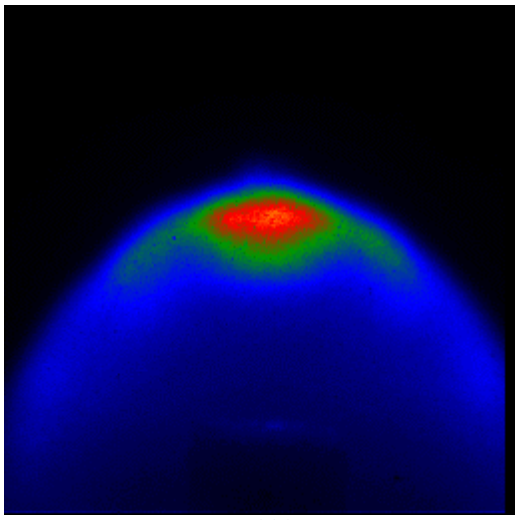

t=800ns

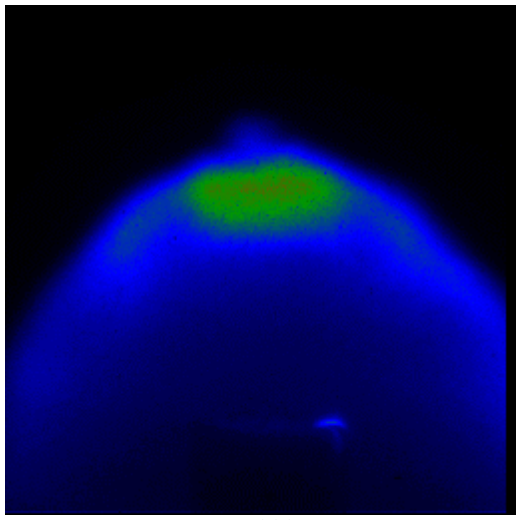

t=1000ns

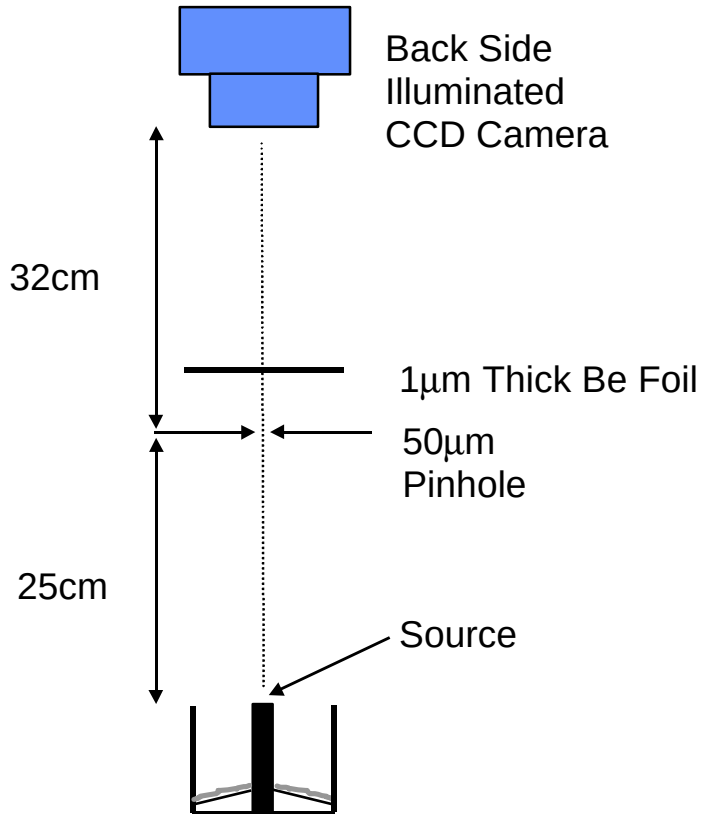

Fig 9 Pin hole camera arrangement used for taking EUV images.

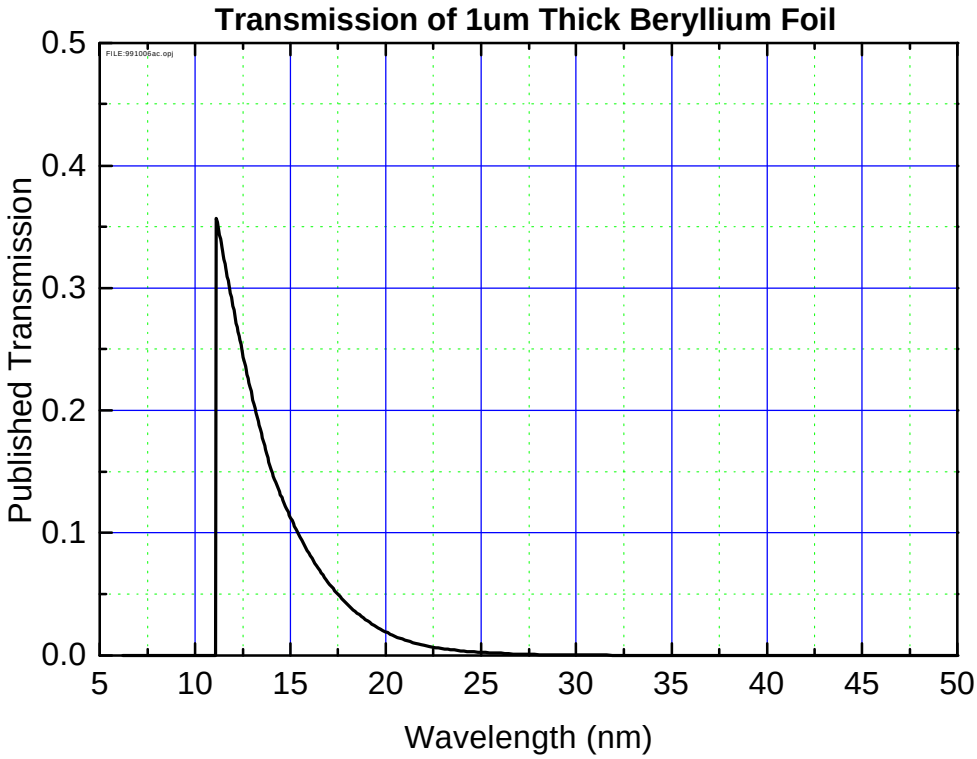

Fig 10. Published EUV transmission of 1µm thick Beryllium foil.

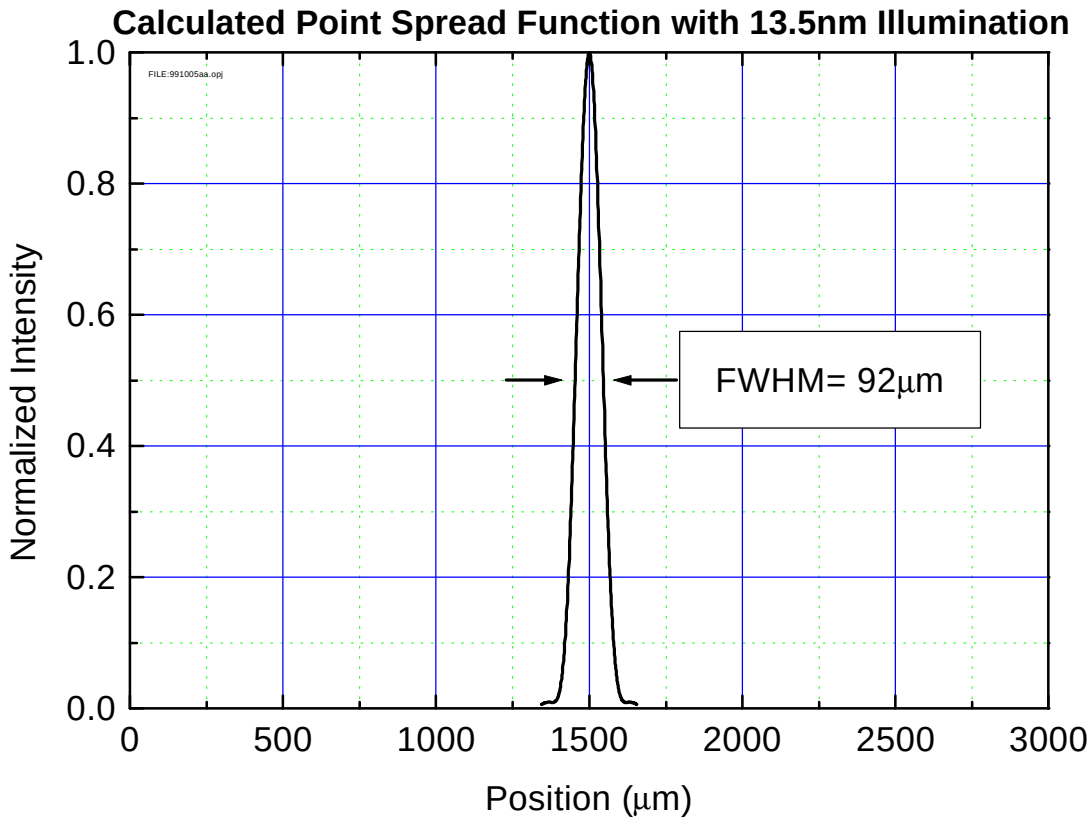

Fig 11. Calculated spatial resolution of pin hole camera.

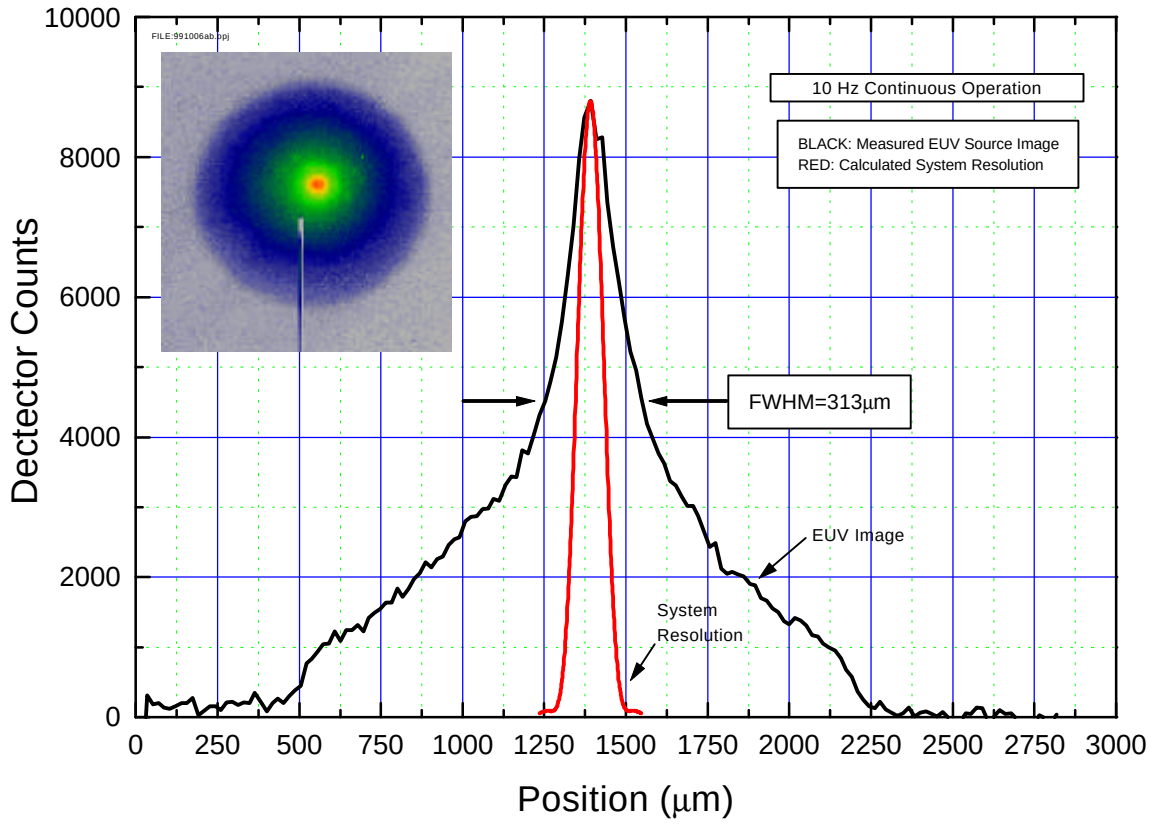

Fig 12. EUV source image taken while operating at 10Hz with an Argon buffer gas.

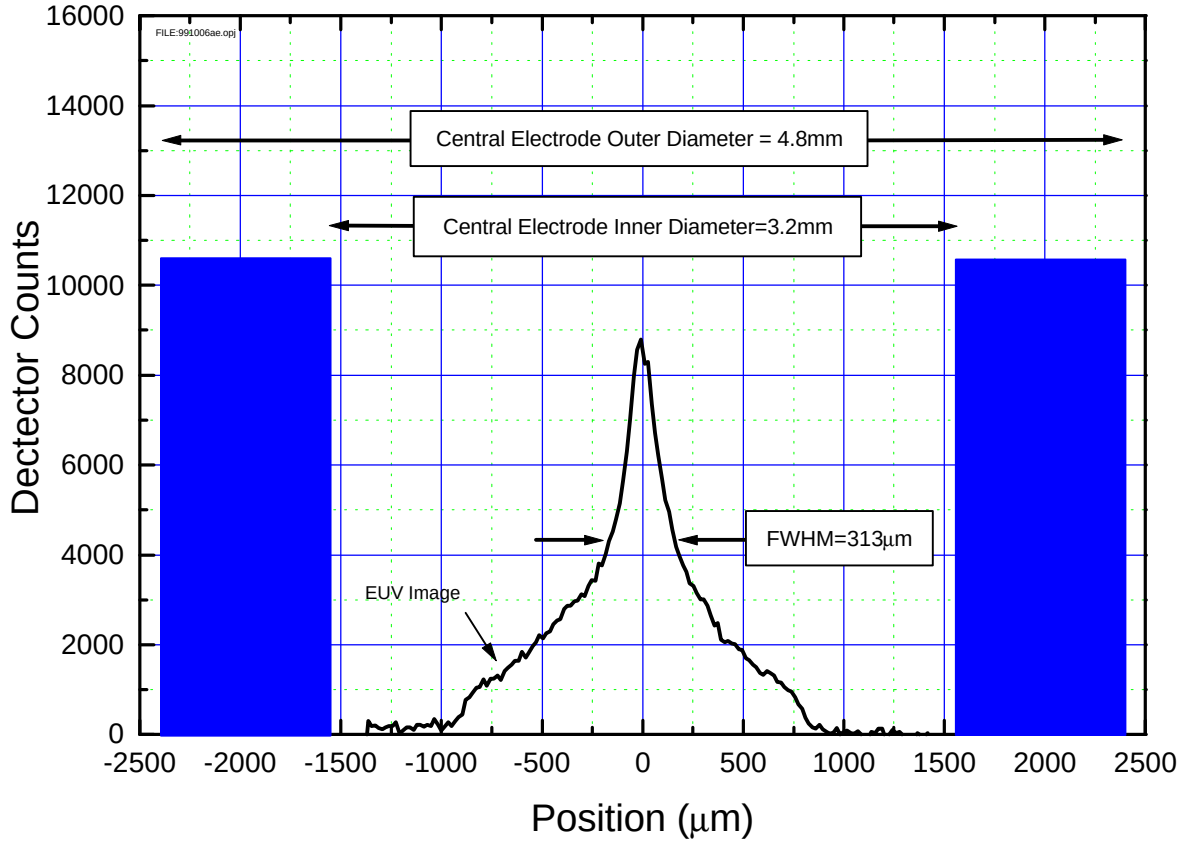

Fig 13. EUV source image plotted relative to the anode dimensions.

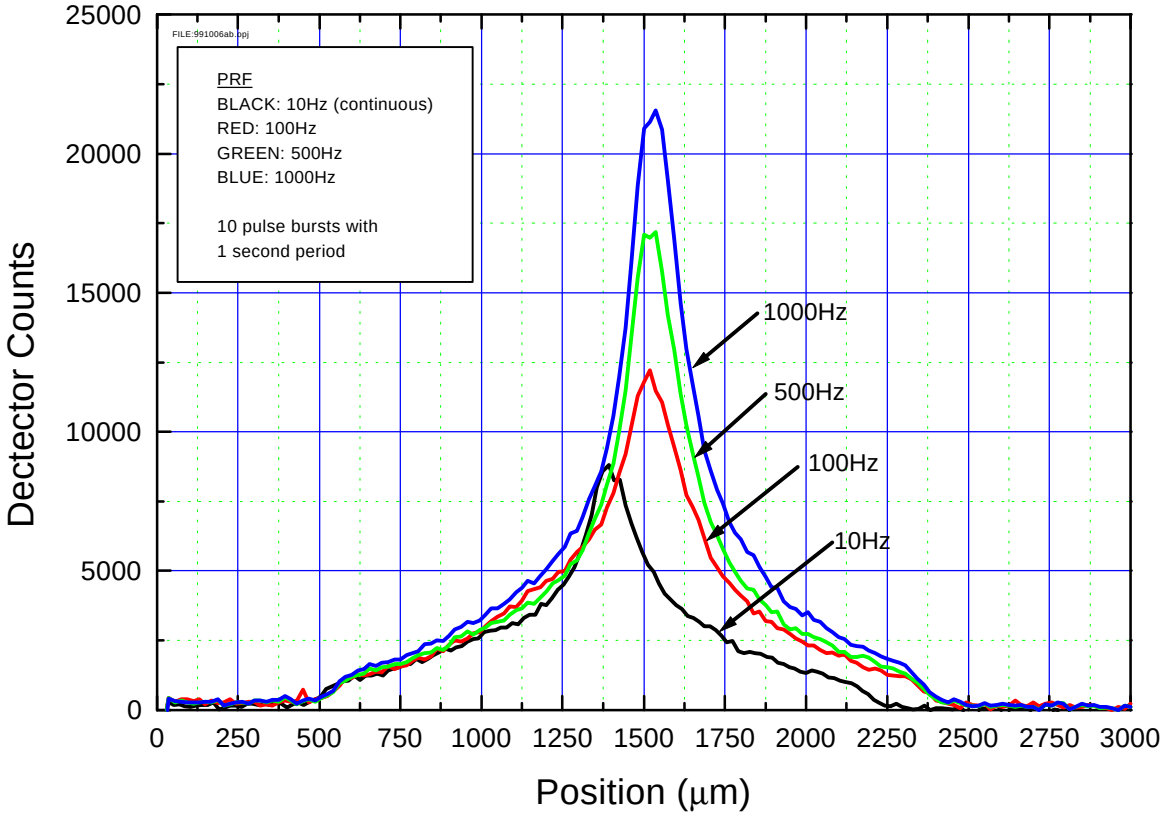

Fig 14. Measured EUV profiles for repetition rates from 10Hz to 1000Hz.

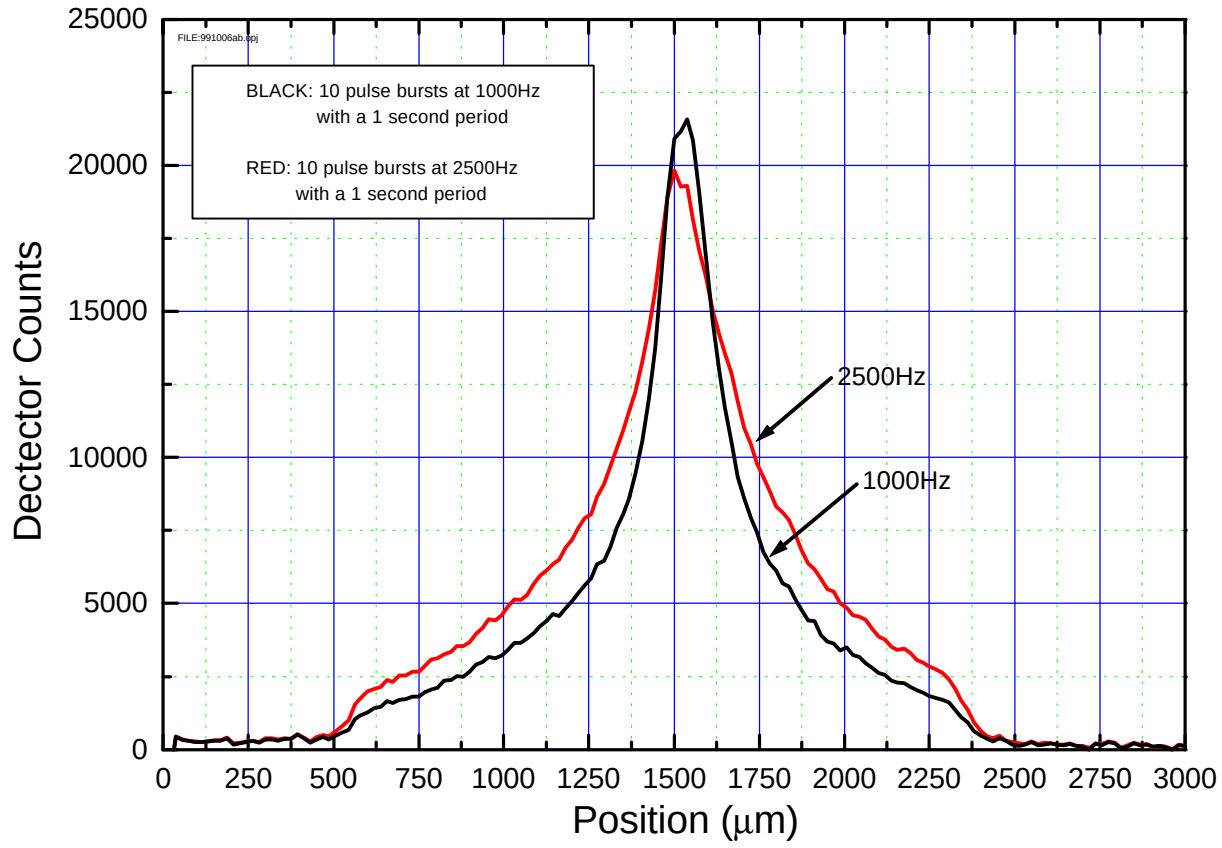

Fig 15. Measured EUV profile for 2500Hz operation with 1000Hz profile for comparison.

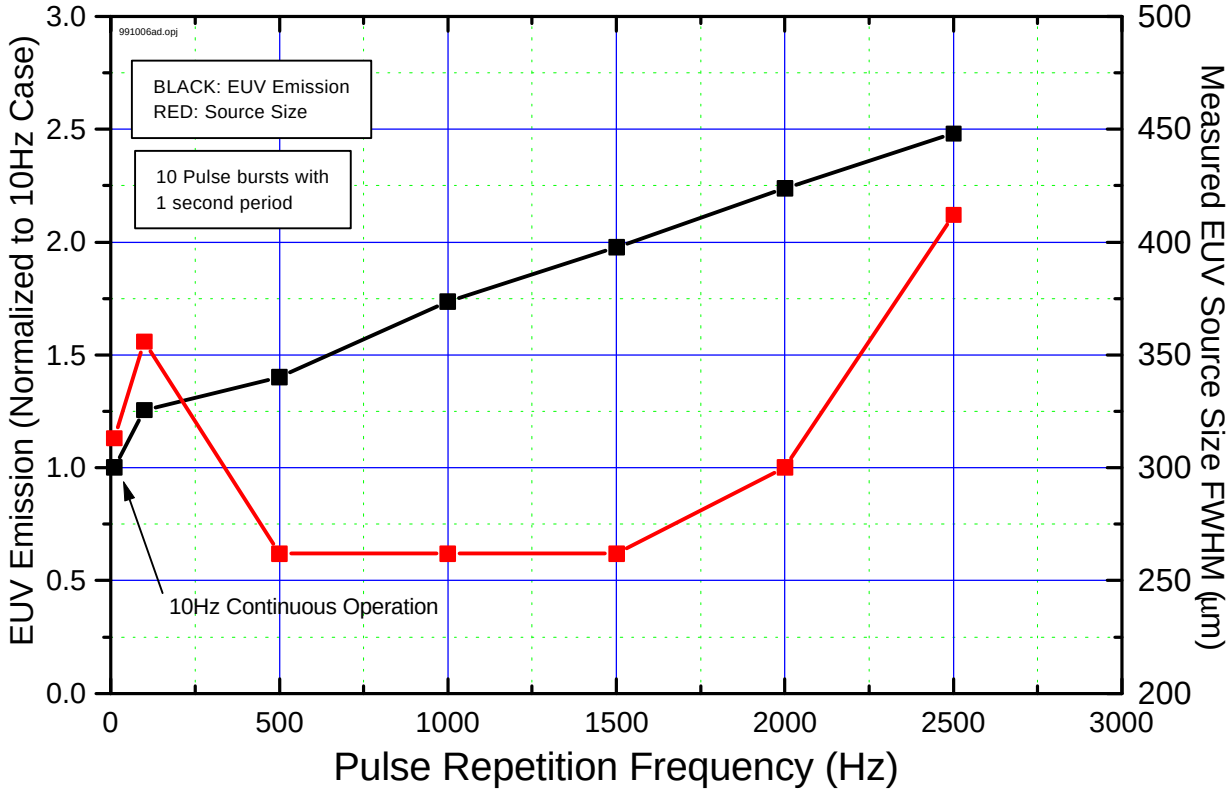

Fig 16. Summary of measured source size and total EUV emission vs. repetition rate.

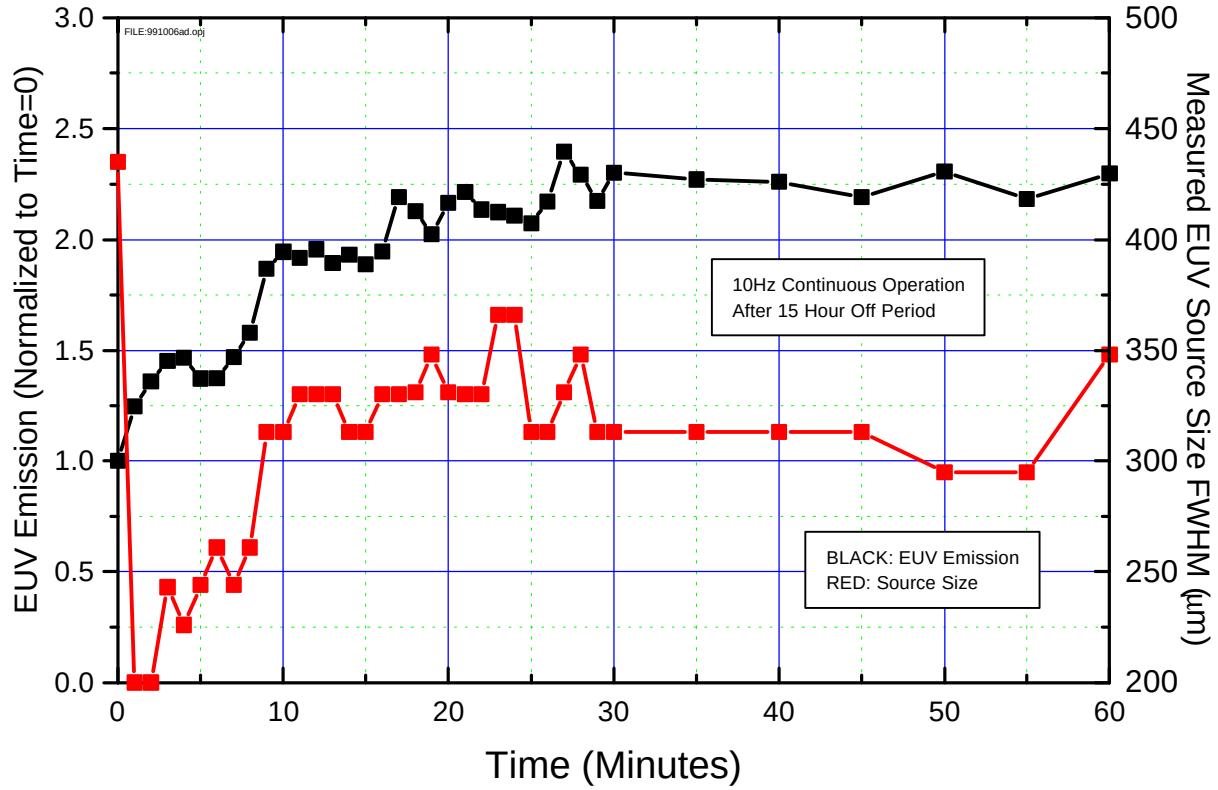

Fig 17. Measured source size and total EUV emission vs. time after 15 hour off period showing 30 minute "warm-up".

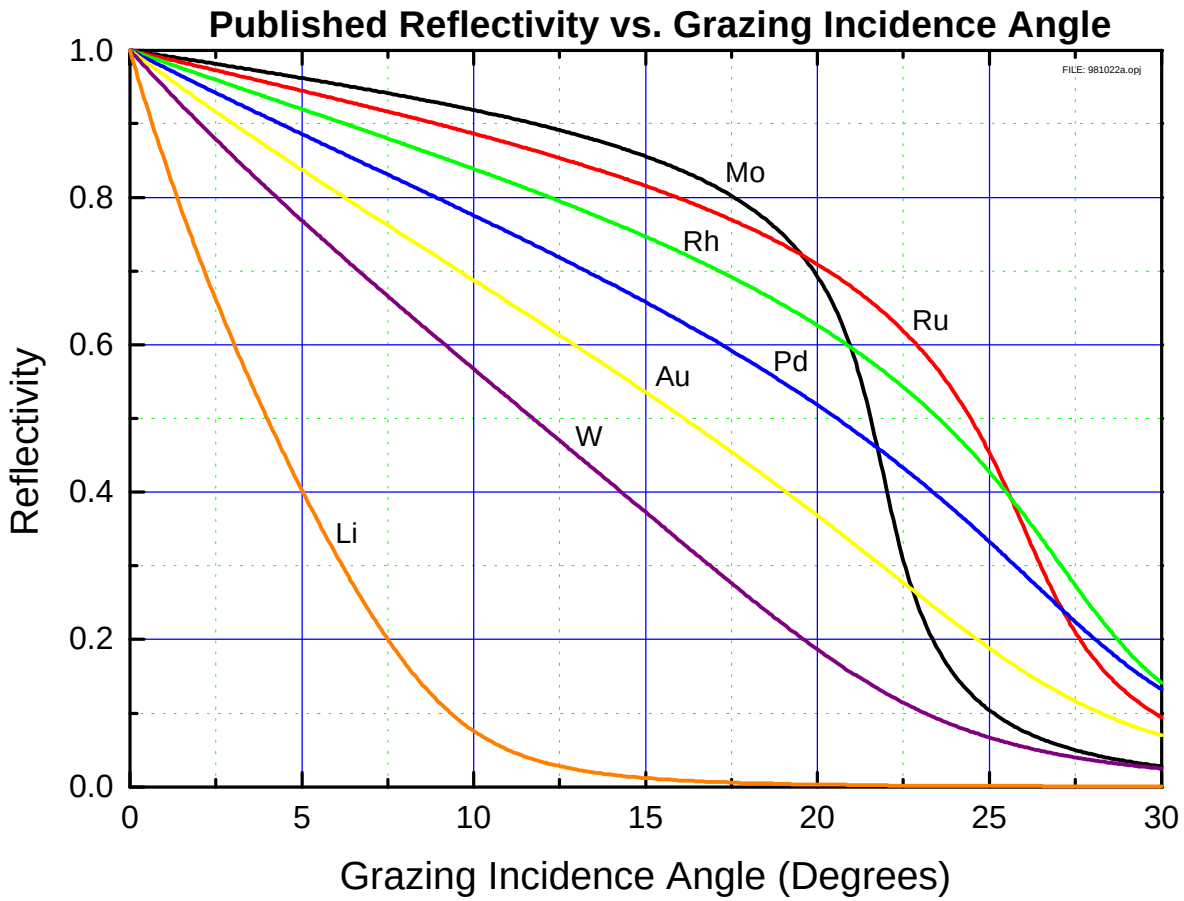

Fig 18. Published 13.5nm reflectivity vs. angle for various candidate grazing incidence plating materials.

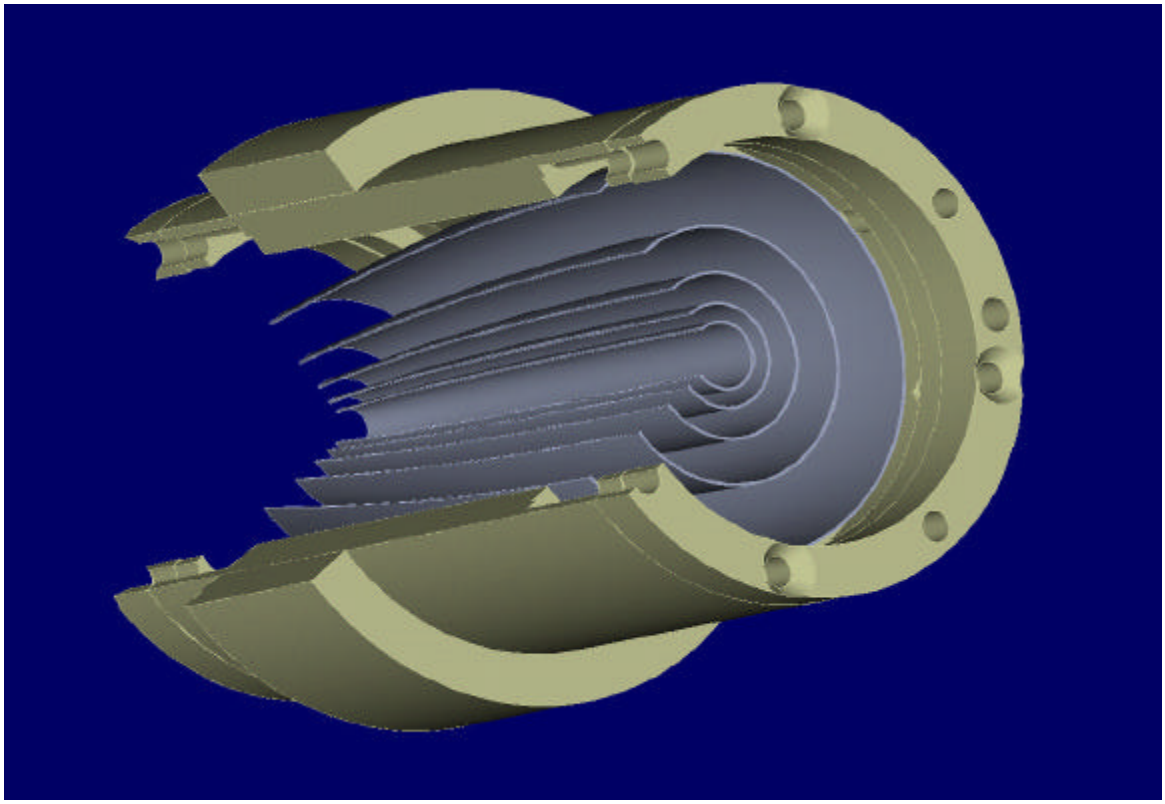

Fig 19. CAD rendering of first prototype grazing incidence collector.

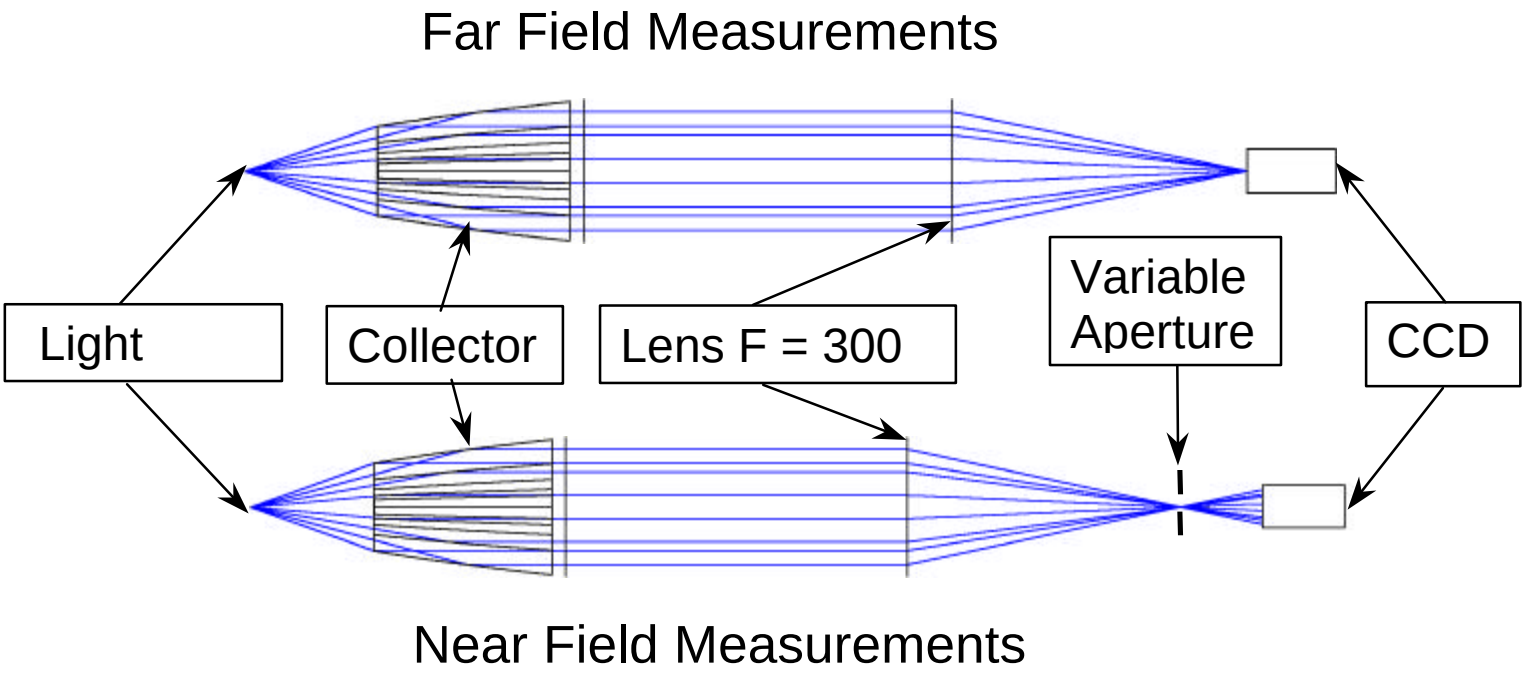

Fig 20. Optical setup used to test grazing incidence collector.

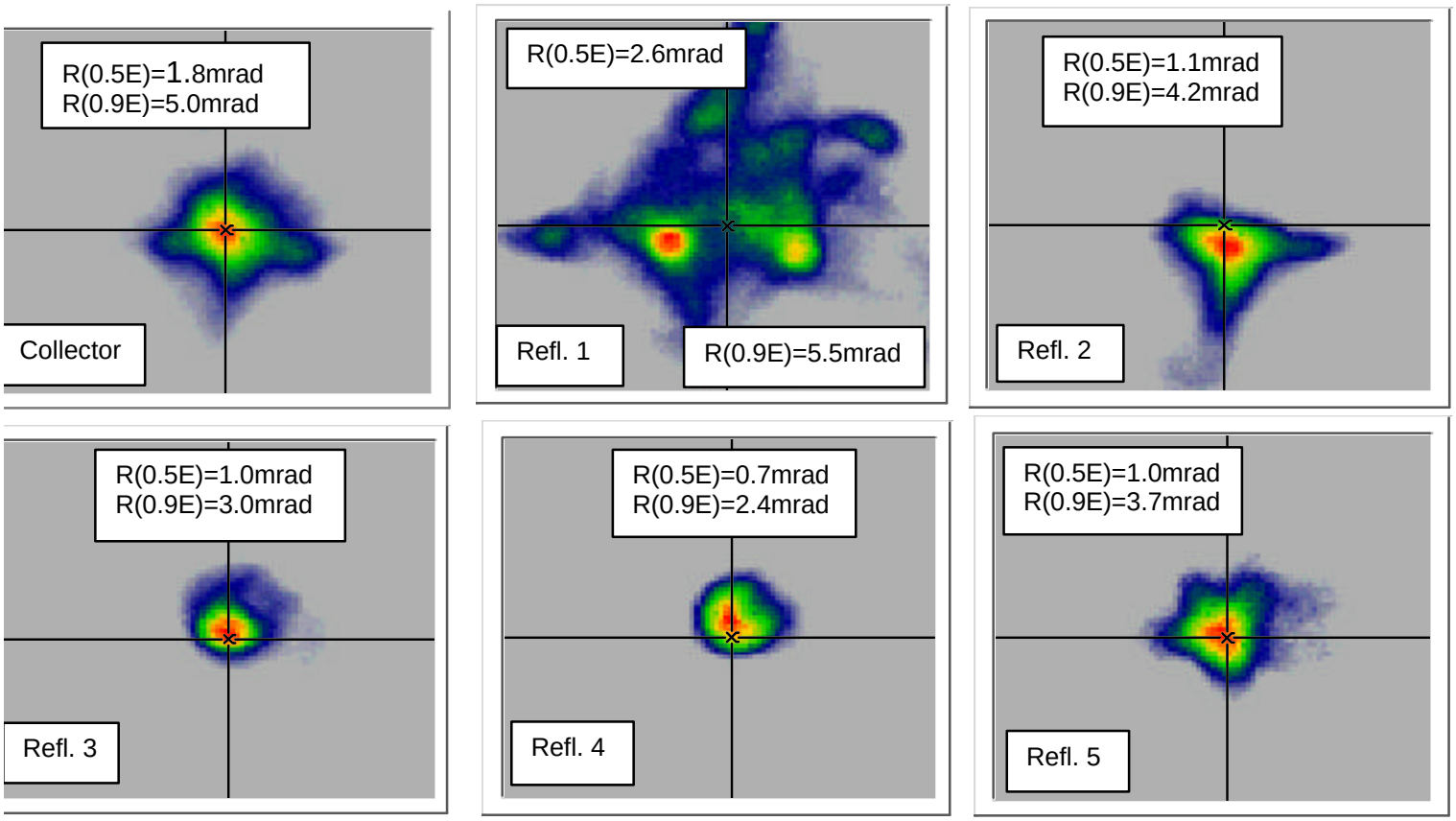

Fig 21. Measured far field performance of prototype grazing incidence collector.

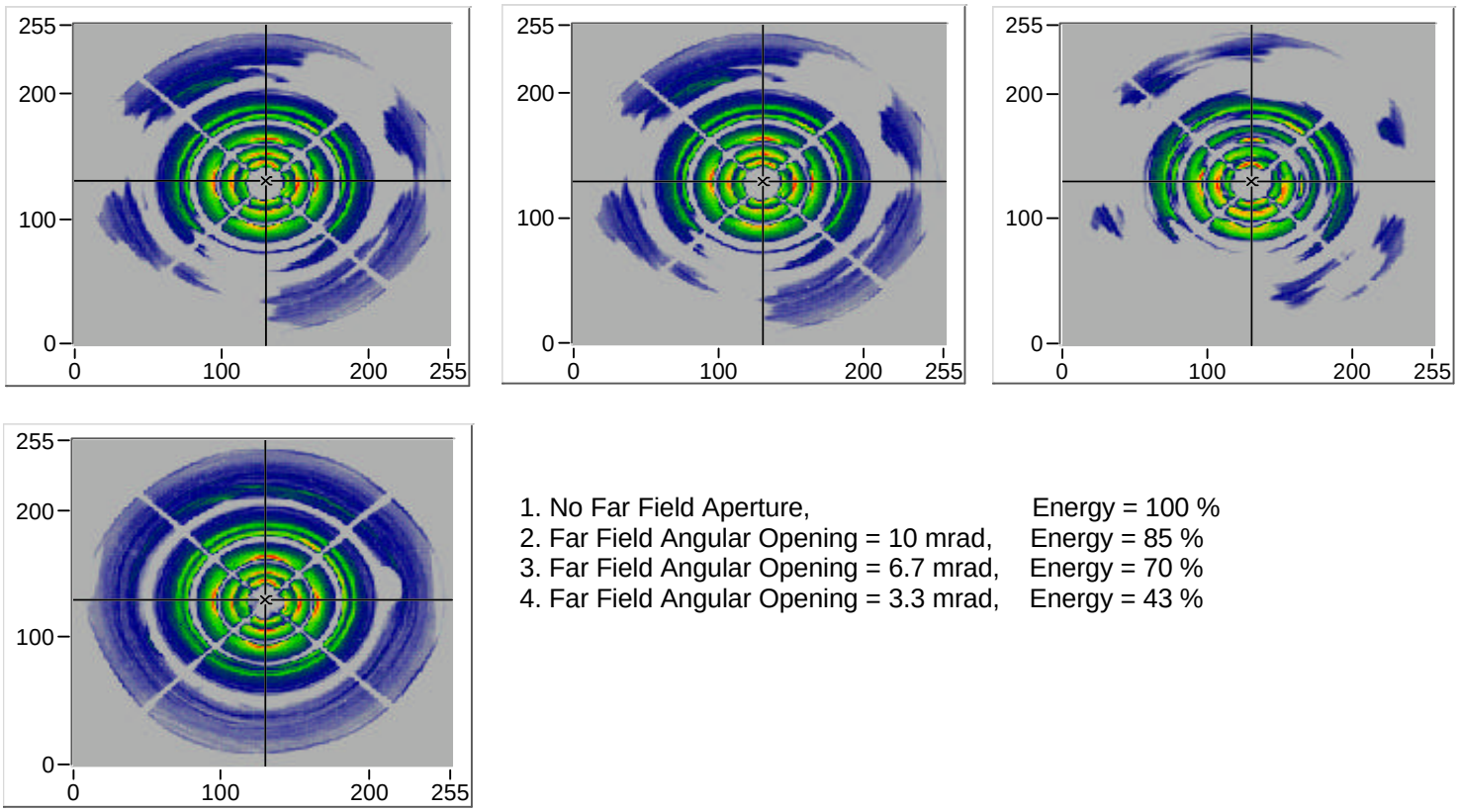

1. No Far Field Aperture, Energy = 100 %
2. Far Field Angular Opening = 10 mrad, Energy = 85 %
3. Far Field Angular Opening = 6.7 mrad, Energy = 70 %
4. Far Field Angular Opening = 3.3 mrad, Energy = 43 %

22. Measured near field performance of prototype grazing incidence collector.

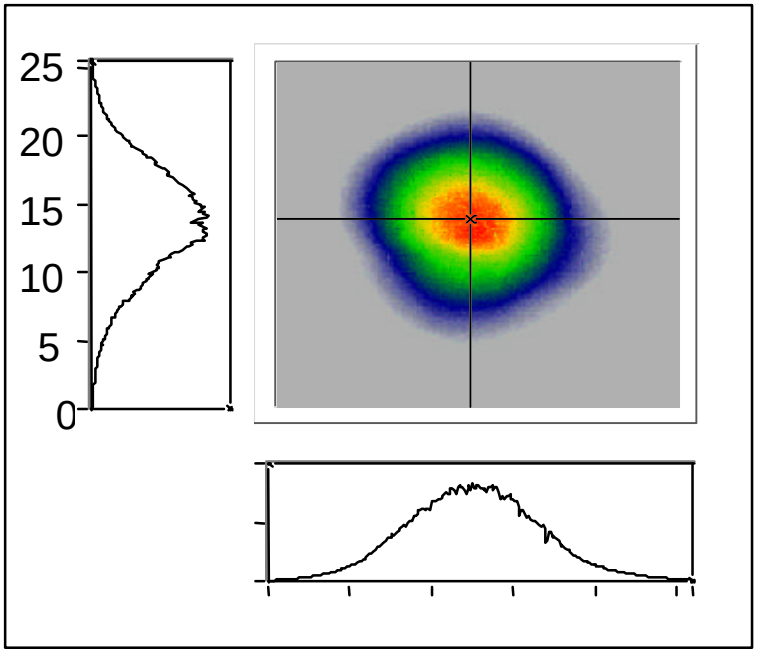

Source Diameter = 0.5mm

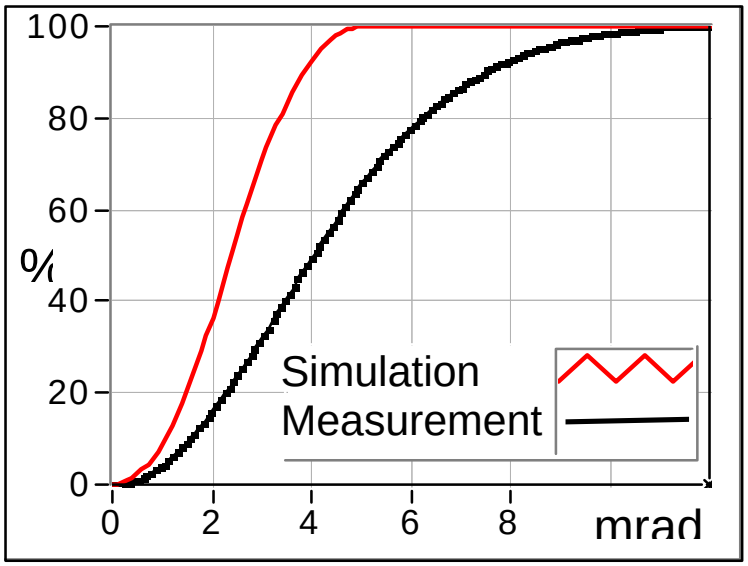

	Sim.	Exp.
Radius of 50 % Energy =	2.4 ;	4.0 mrad
Radius of 90 % Energy =	3.9 ;	7.6 mrad

Fig 23. Measured divergence with 500µm diameter source illumination.